AIAA JOURNAL
Vol. 31, No. 11, November 1993

# Characteristics of Stretched Vortical Structures in Two-Dimensional Stagnation Flow

Chin Yi Wei* and Jiun Jih Miau†
*National Cheng Kung University, Tainan 70101, Taiwan, Republic of China*

**Quantitative aspects on the relationship of the incoming freestream turbulence and the stretched vortical structures developed in a two-dimensional stagnation region are reported in this work. The optimal time delay that resulted from the cross correlation of the velocity fluctuations measured in the stagnation region and the wall-pressure fluctuations is successfully normalized by the freestream velocity and the width of the bluff body, implying that this time delay is attributed to the effect of mean-flow convection. The statistics regarding the unsteady stretched vortical structures detected at a fixed location in the stagnation region, in terms of the number of events per unit time and the averaged time duration of the flow structures detected, are successfully scaled by $L_x$ and $u_0$, where $L_x$ and $u_0$ are the integral length scale and the intensity of grid-generated turbulence, respectively.**

## Nomenclature

$a$ = constant representing the slope of mean streamwise velocity along a two-dimensional stagnation streamline
$D(t)$ = detection function to trigger the conditional sampling procedure
$F$, $G$ = functions employed in dimensional analysis
$f_q$ = statistics of the intermittent events per unit time
$H_v$ = characteristic length scale of the stretched vortical structures
$\hat{i}, \hat{j}, \hat{k}$ = unit vectors in $x$, $y$, and $z$ directions, respectively
$L_x$ = longitudinal integral length scale of freestream turbulence
$M^*_{p_w u}$ = $p^*_w(t + \tau_{\text{opt}})u^*(t)$
$P$, $\tilde{P}$ = time-mean and instantaneous wall pressure, respectively
$P_0$ = stagnation pressure
$p$ = pressure fluctuation
$p_w$ = wall-pressure fluctuation
$q$ = fluctuating velocity measured by a normal hot wire
$Re$ = Reynolds number
$R_{s_A s_B}$ = space-time cross correlation of fluctuating quantities $s_A$ and $s_B$
$s$ = fluctuating quantity
$S_{\text{I}}$, $S_{\text{II}}$, $S_{\text{III}}$ = turbulence-generating screens
$t$ = time
$t_q$ = averaged time duration of the intermittent events detected
$U_0$, $u_0$ = streamwise velocity and streamwise velocity fluctuation in freestream
$U$, $V$, $W$ = mean velocities of $x$, $y$, and $z$ components, respectively
$\tilde{U}$, $\tilde{V}$, $\tilde{W}$ = instantaneous velocity vectors of $x$, $y$, and $z$ components, respectively
$u$, $v$, $w$ = velocity fluctuations in $x$, $y$, and $z$ directions, respectively
$W_d$ = width of plate, 25 mm
$x$, $y$, $z$ = Cartesian coordinates
$\Delta t$ = time delay in cross correlation
$\Delta x$, $\Delta y$, $\Delta z$ = separation distances of two probes in the $x$, $y$, and $z$ directions, respectively
$\lambda_0$ = viscous length scale, $2\pi/\sqrt{(a/\nu)}$
$\nu$ = kinematic viscosity of air
$\rho$ = density of air
$\sigma$ = threshold value of the detection function
$\tau_n$ = normalized optimal time delay
$\tau_{\text{opt}}$ = optimal time delay resulted from cross correlation

*Subscripts and Superscript*

$A$, $B$ = flow quantities at the measured positions $A$ and $B$
$*$ = normalized fluctuating quantity

## I. Introduction

STUDYING the physical aspects of turbulent stagnation flow is relevant to a number of engineering applications, for instance, predictions of the heat transfer rate of heat exchangers[1] and the development of the turbulent boundary layer from the stagnation region.[2] In this research area, the role of the stretched vortical structures present in the stagnation region has attracted the attention of researchers, because the flow structures are capable of enhancing momentum transport as well as heat transfer, thus influencing the fluid-dynamical aspects and heat transfer characteristics of the stagnation flow.

As plausible, the stretched vortical structures detected in the stagnation region have a direct link to the turbulent eddies embedded in the incoming freestream. However, this relationship is not necessarily straightforward. Reports found in the literature indicate that the disturbances amplified in the stagnation region are selective. Nagib and Hodson[3] studied the disturbance generated by a circular cylinder impinged on a two-dimensional bluff body and found a threshold condition for the incipient formation of the vortices in the stagnation region. Sadeh et al.[4,5] presented the theoretical analysis and experimental results to explain the amplification of disturbances convecting toward the stagnation region. They found that if the characteristic length scale of the disturbance is greater than a viscous length scale $\lambda_0$, where $\lambda_0 = 2\pi/\sqrt{(a/\nu)}$, the disturbance is amplified in the stagnation region. Otherwise, the viscous dissipation effect dominates over the vortex-stretching mechanism, and the disturbance is damped as the flow approaches the stagnation region.

Hunt[6] considered a turbulent flow over a bluff body from a standpoint of the rapid-distortion theory.[7] He found that the turbulence intensity is amplified in the stagnation region if the

Received March 24, 1992; revision received Dec. 20, 1992; accepted for publication March 24, 1993. Copyright © 1993 by the American Institute of Aeronautics and Astronautics, Inc. All rights reserved.

*Graduate Student, Institute of Aeronautics and Astronautics; currently Associate Professor, Department of Aeronautics, Chinese Air Force Academy, Kangshaw, Kaosiung, Taiwan, Republic of China.
†Professor, Institute of Aeronautics and Astronautics.

characteristic length scale of the freestream turbulence, denoted as $L_x$, is much smaller than the characteristic dimension of the bluff body, denoted as $W_d$; namely, the mechanism of vorticity stretching is dominant. On the other hand, the turbulence intensity is damped in the stagnation region if $L_x$ is much greater than $W_d$; namely, the blocking effect they identified is dominant. In the latter case, the turbulent fluctuations act as an unsteady mean flow varying in magnitude and direction to the bluff body. Theoretical predictions of Hunt[6] are confirmed by the experimental results of Bearman[8] and Britter et al.[9]

Previously, the present authors[10] made efforts to describe the characteristics of the stretched flow structures in the stagnation region quantitatively in terms of the properties of the incoming freestream turbulence. A marked finding is that the characteristic length scale of the stretched flow structures deduced from the velocity correlation measurements is proportional to the integral length scale of the incoming turbulence, provided that the integral length scale satisfies both criteria of Hunt[6] and Sadeh et al.[4,5] for vorticity amplification. This finding enlightens a practical application that if one knows the characteristics of freestream turbulence, one could further predict the behaviors of the stretched vortical structures in the stagnation region. The present work is a further attempt in this direction to explore the unsteady characteristics of the stretched flow structures in the stagnation region that will be described by the parameters of the freestream turbulence.

## II. Experimental Method

Experiments were conducted in a closed-return low-speed wind tunnel with a test section 28 × 45 cm in cross section and 100 cm in length. A flat plate 50 mm in width, denoted as $W_d$, and 280 mm in length was placed normal to the flow for producing a two-dimensional stagnation flowfield. This plate was spanned vertically between the walls of the test section and was fitted with a profiled afterbody, 60 mm at its maximum width and $4W_d$ in length. This afterbody served for suppressing vortex shedding downstream of the bluff body, thus eliminating the velocity fluctuations in the region upstream of the plate that could be induced by the shedding vortices in the wake.[11] The configuration of the bluff body and the coordinate system employed are shown in Fig. 1. In this study, the Reynolds number is defined as $Re = (U_0 W_d/\nu)$, which ranges from $1 \times 10^4$ to $3.2 \times 10^4$.

The freestream condition of the flow was controlled by a turbulence-generating screen situated at the inlet of the test section. Three kinds of screens were selected for the present purpose, denoted as $S_{\mathrm{I}}$, $S_{\mathrm{II}}$, and $S_{\mathrm{III}}$. Both $S_{\mathrm{I}}$ and $S_{\mathrm{II}}$ were the square-mesh woven screens with wire diameter of 0.8 and 2.4 mm, respectively. The mesh sizes of the screens $S_{\mathrm{I}}$ and $S_{\mathrm{II}}$ were 12.7 and 30.0 mm, respectively, corresponding to the open area ratios of 0.88 and 0.85. The screen $S_{\mathrm{III}}$ was made with strips of tape 12.5 mm in width taped over a diamond-shaped mesh screen whose mesh size and wire diameter were 11.5 and 0.9 mm, respectively. Please refer to Wei and Miau[10] for a schematic drawing of $S_{\mathrm{III}}$. The open area ratio of the screen $S_{\mathrm{III}}$ was 0.52. This screen could produce turbulence whose intensity and characteristic length scale were much larger than those produced by $S_{\mathrm{I}}$ and $S_{\mathrm{II}}$. The turbulence intensity measured at the location of the normal plate was 0.3% of the freestream velocity, when the plate and the turbulence-generating screen were absent from the flowfield.

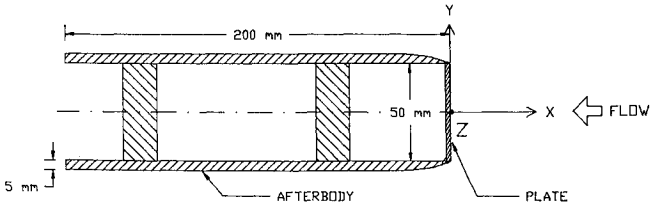


**Fig. 1 Schematic view of the plate attached by a profiled afterbody and the coordinate system employed.**

**Table 1 Freestream turbulence intensity and longitudinal integral length scale for arrangements I–VI obtained at $U_0 = 3.1$ and 9.6 m/s**

| Arrangement | $U_0$, m/s | $\overline{u^2}^{1/2}/U_0$, % | $\overline{v^2}^{1/2}/U_0$, % | $\overline{w^2}^{1/2}/U_0$, % | $L_x$, mm |
|---|---|---|---|---|---|
| I | 3.1 | 1.3 | 1.1 | 1.1 | 7.42 |
| I | 9.6 | 1.3 | 1.1 | 1.1 | 6.11 |
| II | 3.1 | 2.7 | 2.2 | 2.2 | 9.18 |
| II | 9.6 | 2.8 | 2.2 | 2.2 | 9.78 |
| III | 3.1 | 7.4 | 6.3 | 6.1 | 21.16 |
| III | 9.6 | 8.0 | 7.3 | 7.1 | 20.43 |
| IV | 3.1 | 1.8 | 1.5 | 1.5 | 5.94 |
| IV | 9.6 | 1.9 | 1.7 | 1.7 | 5.17 |
| V | 3.1 | 3.8 | 3.2 | 3.2 | 7.85 |
| V | 9.6 | 3.3 | 2.8 | 2.8 | 8.74 |
| VI | 3.1 | 11.6 | 10.8 | 10.6 | 18.08 |
| VI | 9.6 | 11.9 | 11.0 | 10.8 | 20.25 |

The experimental arrangements I, II, and III described in the following refer to when the normal plate was situated 62 cm downstream of screens $S_{\mathrm{I}}$, $S_{\mathrm{II}}$, and $S_{\mathrm{III}}$, respectively; the arrangements IV, V, and VI refer to when the plate was situated 40 cm downstream of screens $S_{\mathrm{I}}$, $S_{\mathrm{II}}$, and $S_{\mathrm{III}}$, respectively. The turbulence intensity and the integral length scale measured at the location of the plate for each of the arrangements, while the plate was absent from the flowfield, are listed in Table 1. In this table, the freestream turbulence levels corresponding to the cases studied vary in a range of 1.3–11.9%, and the corresponding integral length scales $L_x$ vary in a range of 5.17–21.96 mm, i.e., about $0.1$–$0.44W_d$. It is found that the values of $L_x$ corresponding to the six arrangements studied largely fall into the range that satisfies the criterion suggested by Hunt,[6] Sadeh and Brauer,[2] and Sadeh et al.,[4,5] which can be summarized in an expression that $\lambda_0 < L_x \ll W_d$. Nevertheless, the ratios of $L_x/W_d$ corresponding to the arrangements III and VI are larger than 0.4, which cannot be regarded as very small compared with 1. Consequently, according to Hunt,[6] a comparatively weaker effect of vortex stretching in the stagnation region is expected for these cases. For arrangements III and VI, because the ratios of the distance between the screen of $S_{\mathrm{III}}$ and the plate to the characteristic mesh size of the screen are only 10.78 and 6.96, respectively, the turbulent flows developed at the location of the normal plate are expected to be far from homogeneous.[12]

As far as the nonuniformity of the mean-flow distribution in the test section is concerned, when the normal plate was absent from the flow, the streamwise velocity distribution measured at the cross-sectional plane of the normal plate indicated that the nonuniformity was less than 1% for arrangements I and IV, less than 2% for arrangements II and V, and less than 5% for arrangement III, but more than 7% for arrangement VI. As seen, the expense of obtaining the larger length scale of $L_x$ with the screen $S_{\mathrm{III}}$ was to increase the turbulence intensity and the spatial nonuniformity in the velocity distribution.

A hot-wire probe with straight-tube support was introduced in the region upstream of the normal plate to perform velocity measurement; see Wei and Miau[10] for further details. An $x$-type hot-wire probe was employed to measure the instantaneous velocities in the $x$ and $y$ directions or in the $y$ and $z$ directions by rotating the probe 90 deg. A traversing mechanism was situated on one side of the test section, which moved the hot-wire probe to desirable positions. The resolution of traversing was 1/66 mm along the horizontal axis and 1/40 mm along the vertical axis.

A pressure-response-type microphone, Bruel & Kjaer No. 4136, was adopted to measure the pressure fluctuations on the surface of the plate. A pinhole 1 mm in diameter was led from the rear surface of the plate to a cavity that was designed to accommodate the microphone probe 6.4 mm in diameter. A schematic drawing of the cavity-mounted microphone transducer is shown in Fig. 2.

Background acoustic noise in the wind tunnel was checked before conducting the experiment. The most significant com-

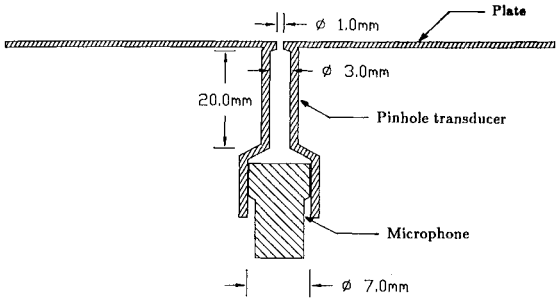


**Fig. 2 Schematic of the cavity-mounted pinhole microphone transducer.**

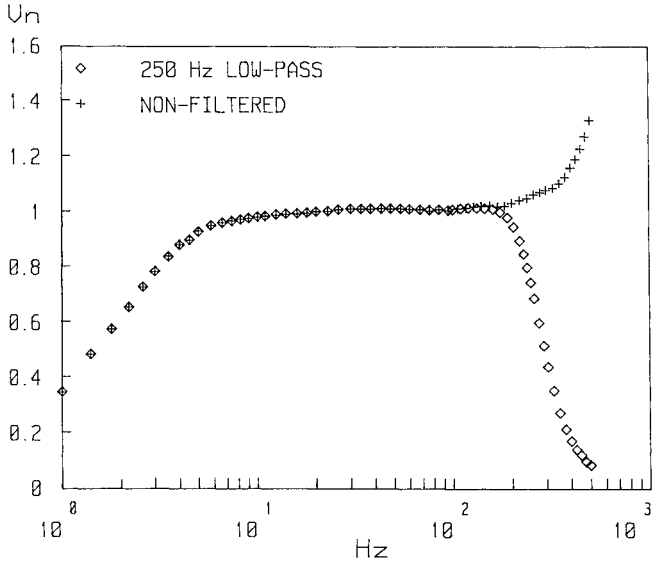


**Fig. 3 Frequency responses of the cavity-mounted pinhole microphone with and without a 250-Hz low-pass filtering process; $V_n$ denotes the normalized output voltage of the microphone.**

ponent in the acoustic noise measured was about 310 Hz, which was identified due to the fan of the wind tunnel. Furthermore, since more than 95% of the energy of the fluctuating signal measured resided below 200 Hz if $U_0 \leq 7.6$ m/s or below 220 Hz if $U_0 \leq 9.6$ m/s, a low-pass filter with a cutoff frequency at 250 Hz was adopted to filter out the acoustic noise at about 310 Hz.

The microphone sensed acoustic noise at about 66 Hz if the experiment was conducted at $U_0 > 11$ m/s, which was identified due to the vibration of the wall of the wind tunnel. This low-frequency noise was impossible to filter out because it fell in the useful range of the signal measured. Thus, the operating velocity of the wind tunnel was limited below 9.6 m/s.

A microphone calibrator, Bruel & Kjaer No. 4221, was employed to calibrate the microphone. The frequency ranges corresponding to the linear output of the microphone, without and with the pinhole transducer, were found to fall in the ranges of 3 Hz to 50 kHz and 5Hz to 230 Hz, respectively. If the microphone was mounted with a pinhole transducer and its output was further low passed by a filter with the cutoff frequency at 250 Hz, the linear range of the frequency response was reduced to within 5–200 Hz; see Fig. 3.

## III. Cross-Correlation Measurement

The space-time cross-correlation measurements were conducted to study the behavior of the large-scale vortical structures developed in the stagnation region. The space-time correlation under consideration is defined by

$$R_{s_A s_B}(\Delta x, \Delta y, \Delta z, \Delta t) = \frac{\overline{s_A(x_A, y_A, z_A, t_0) s_B(x_B, y_B, z_B, t)}}{\sqrt{\overline{s_A^2}}\sqrt{\overline{s_B^2}}} \quad (1)$$

where the spatial separation of the two probes is defined by $\Delta x = x_B - x_A$, $\Delta y = y_B - y_A$, and $\Delta z = z_B - z_A$; $\Delta t$ denotes the time lag between the two signals for correlation; and the overbar denotes the time average. Since the measured positions $A$ and $B$ are not shown explicitly on the left-hand side of Eq. (1), in the later presentation of the correlation results the measured positions will be described along with the data given.

Correlation measurements of the wall-pressure fluctuations and the velocity fluctuations obtained with a normal hot-wire aligned in the $z$ direction, denoted as $R_{p_w q}(\Delta x, 0, 0, \Delta t)$, were carried out at the sections $y = 8$, 12, 16, and 20 mm. Selection of these $y$ sections for correlation measurements was based on the following considerations. First, earlier measurements[10] of $R_{q_A q_B}(0, \Delta y, 0, 0)$ obtained by two normal hot wires situated at a cross-sectional plane of constant $x$, mounted symmetrically with respect to the mean stagnation streamline, indicated that the stretched flow structures developed in the stagnation region were orientated essentially in the $y$ direction. This can also be seen from the isocontours of $R_{q_A q_B}(0, \Delta y, 0, 0)$ in Fig. 4, which is reproduced from Wei and Miau.[10] For a fixed separation of two normal hot wires, $\Delta y$, the isocontours presented in Fig. 4 show a tendency for the correlation values to increase as flow approaches from freestream to a location $x = H_v$. In Wei and Miau,[10] the distance $H_v$ measured from the wall is referred to as a characteristic length of the stretched vortical structures

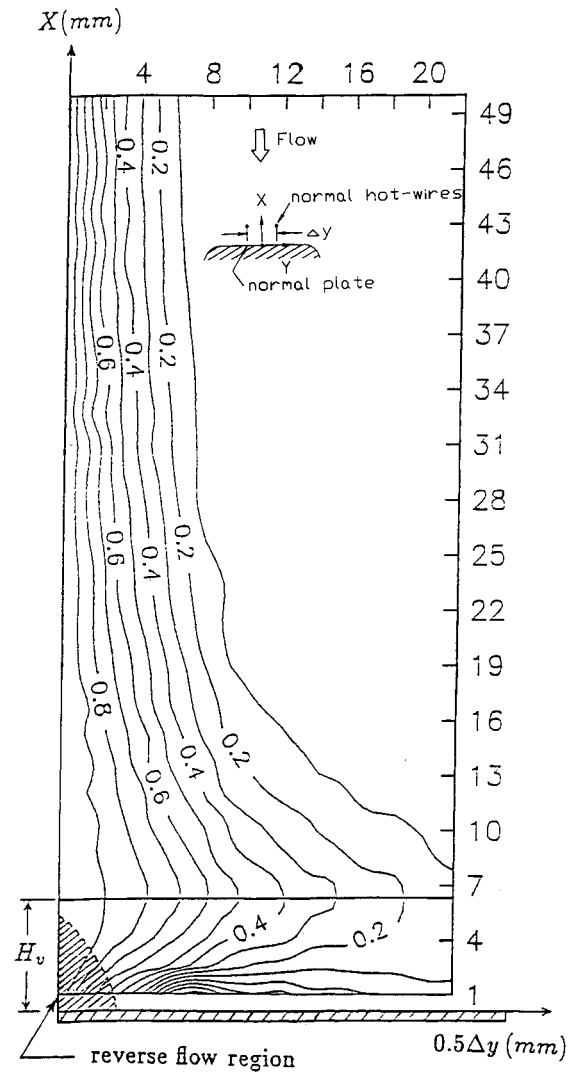


**Fig. 4 Isovalue contours of $R_{q_A q_B}(0, \Delta y, 0, 0)$ for arrangement II at $U_0 = 3.1$ m/s (Ref. 10). Two normal hot-wire probes are situated symmetrically with respect to the mean stagnation streamline. The horizontal axis indicates half the separation distance of the two hot-wire probes, ½Δy.**

in the stagnation region, and $x = H_v$ signifies a time-mean position at which the incoming turbulence eddies are stretched to an ultimate situation. Thus, in the neighborhood of $x = H_v$, the signature of the stretched flow structures is detectable at a certain distance away from $y = 0$. Second, it is found that the presence of a hot-wire probe may influence the wall-pressure signal $p_w$ measured if the hot-wire probe and the pressure tap are situated at a $y$ section for which $y < 6$ mm. At $y > 6$ mm, the characteristic of the wall-pressure signal measured was found to be unaffected by the presence of the hot-wire probe. Third, the measured region should not be situated too far away from the mean stagnation streamline, otherwise the flow characteristics measured might be affected by the flow development at the edge of the normal plate.

Correlation measurements of wall-pressure fluctuations and each component of the velocity fluctuations, namely, $R_{p_w u}(\Delta x, 0, 0, \Delta t)$, $R_{p_w v}(\Delta x, 0, 0, \Delta t)$, and $R_{p_w w}(\Delta x, 0, 0, \Delta t)$, were also performed with an $x$-type hot-wire probe located at the section $y = 16$ mm, for $x$ varying from 2 to 8 mm. Velocity measurement with the $x$-type probe situated farther away from the wall, i.e., $x > 8$ mm, could result in significant error due to the large incident angle of the incoming flow.

## IV. Results and Discussion

### A. Characteristics of Cross-Correlation of $u^*$ and $v^*$

The instantaneous velocity fluctuations measured by an $x$-type hot-wire probe near the wall are reduced into two components in the $x$ and $y$ directions, called $u^*$ and $v^*$, respectively, where $u^*$ and $v^*$ denote the quantities normalized by their root-mean-square values. The distributions of the correlation coefficients of $u^*v^*$ obtained at $y = 16$ mm for $U_0 = 3.1$, 5.0, and 7.6 m/s are shown in Fig. 5a. Notably, the values obtained in the region of $3 < x < 8$ mm are negative. In addition, a typical time trace of $u^*v^*$ obtained at $x = 6$ mm is shown in Fig. 5b and reveals that negative values of $u^*v^*$ occurred most of the time and that there are intermittent events corresponding to large negative peak values. Literally speaking, these intermittent events imply two possible situations: 1) if $u^*$ is negative and $v^*$ is positive, the accelerating flow is sweeping toward the wall; and 2) if $u^*$ is positive and $v^*$ is negative, the decelerating flow was deflected away from the wall. These flow behaviors will be considered further later.

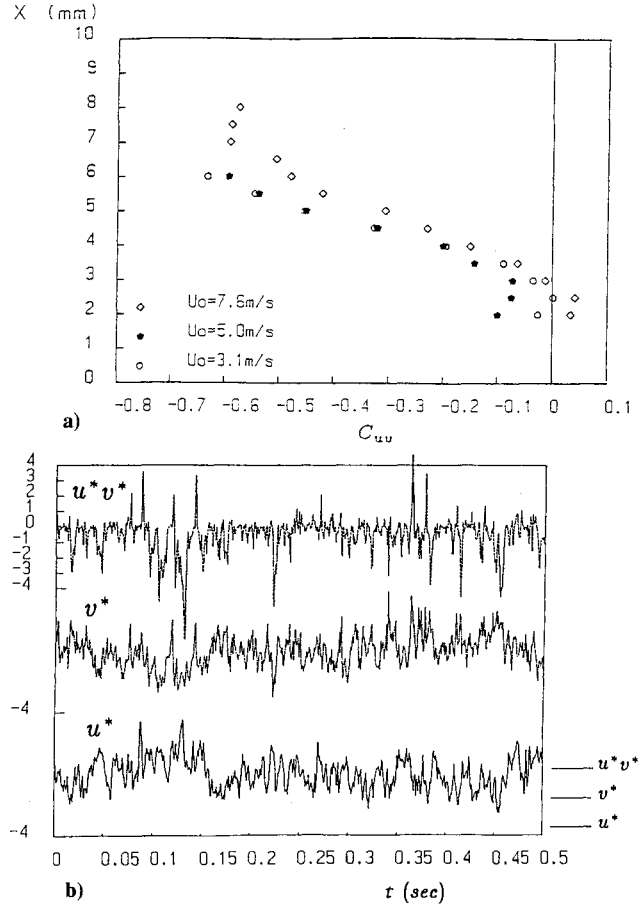


**Fig. 5 Characteristics of the $u^*v^*$ correlation for arrangement II: a) the correlation coefficients measured at $y = 16$ mm and $U_0 = 3.1$, 5.0, and 7.6 m/s and b) the typical time traces of $u^*$, $v^*$, and $u^*v^*$ measured at $x = 6$ mm and $y = 16$ mm for $U_0 = 9.6$ m/s.**

### B. Cross Correlation of Wall-Pressure Fluctuation and Velocity Fluctuation

Since the location of the pressure tap on the wall and the location of an $x$-type hot-wire probe in the flowfield are separated by a distance $\Delta x$, it is plausible that to tune the measured wall-pressure and the velocity fluctuation traces may require a time shift. This time shift is termed "the optimal time delay" in the following, denoted $\tau_{opt}$.

Figure 6 presents a set of the distributions of $R_{p_w u}(\Delta x, 0, 0, \Delta t)$, $R_{p_w v}(\Delta x, 0, 0, \Delta t)$, and $R_{p_w w}(\Delta x, 0, 0, \Delta t)$, for arrangement II at $U_0 = 9.6$ m/s, where the $x$-type probe was located at $y = 16$ mm and $x = 2$, 4, and 6 mm and in the freestream, respectively. A positive peak value read from each of the distributions of $R_{p_w u}(\Delta x, 0, 0, \Delta t)$ signifies the occurrence of $R_{p_w u}(\Delta x, 0, 0, \tau_{opt})$, whereas a negative peak value read from each of the distributions of $R_{p_w v}(\Delta x, 0, 0, \Delta t)$ signifies the occurrence of $R_{p_w v}(\Delta x, 0, 0, \tau_{opt})$. These appearances further suggest that the induced wall-pressure fluctuations tend to be of the same sign as those of the velocity fluctuations measured in the $x$ direction, but of the opposite sign to those of the velocity fluctuations measured in the $y$ direction. Further, it is interesting to note that the optimal time delay $\tau_{opt}$ read from the curve of $R_{p_w u}(\Delta x, 0, 0, \Delta t)$ does not necessarily coincide with that read from the curve of $R_{p_w v}(\Delta x, 0, 0, \Delta t)$, although the velocity fluctuations of $u$ and $v$ were obtained at the same location; for instance, see the distributions of $R_{p_w u}$ and $R_{p_w v}$ obtained at $x = 4$ mm. This discrepancy implies that the phase delays between $p_w$ and $u$ and between $p_w$ and $v$ are not necessarily the same.

The value of $R_{p_w u}(\Delta x, 0, 0, \tau_{opt})$ measured in the region of $x = 2$–6 mm may reach as high as 0.5, indicating a strong correlation between the signals of $p_w(t + \tau_{opt})$ and $u(t)$. Furthermore, the values of $\tau_{opt}$ obtained at different cross-sectional planes reveal a trend to increase with $x$, for $x = 2$–6 mm. This behavior can be explained by the effect of the mean-flow convection later.

Because the vortical structures developed in a two-dimensional stagnation flow exhibit no preference in the $z$ direction, the curves of $R_{p_w w}(\Delta x, 0, 0, \Delta t)$ shown in the figure indicate no pronounced peak values.

The distributions of $R_{p_w u}$, $R_{p_w v}$, and $R_{p_w w}$ corresponding to the case of the hot wire situated in the freestream show very small correlation values. This appearance further evidences that the wall-pressure fluctuations measured are associated with the stretched vortical structures developed in the near-wall region.

### C. Analysis of Pressure Fluctuation in the Flow

Although the instantaneous pressure fluctuation in a turbulent flowfield is difficult to measure, the qualitative behavior of this quantity in the present flow can be discussed with an inviscid analysis as follows.

For a stagnation flow outside the boundary layer, it is assumed that the turbulence intensity does not affect the distribution of the mean flow.[13] Thus, by assuming that the Bernoulli equation holds for the instantaneous flow,

$$\frac{\tilde{P}}{\rho} + \frac{1}{2}(|\tilde{U}|^2 + |\tilde{V}|^2 + |\tilde{W}|^2) = \frac{P_0}{\rho} \tag{2}$$

where $\tilde{P} = P + p$, and the three components of the instanta-

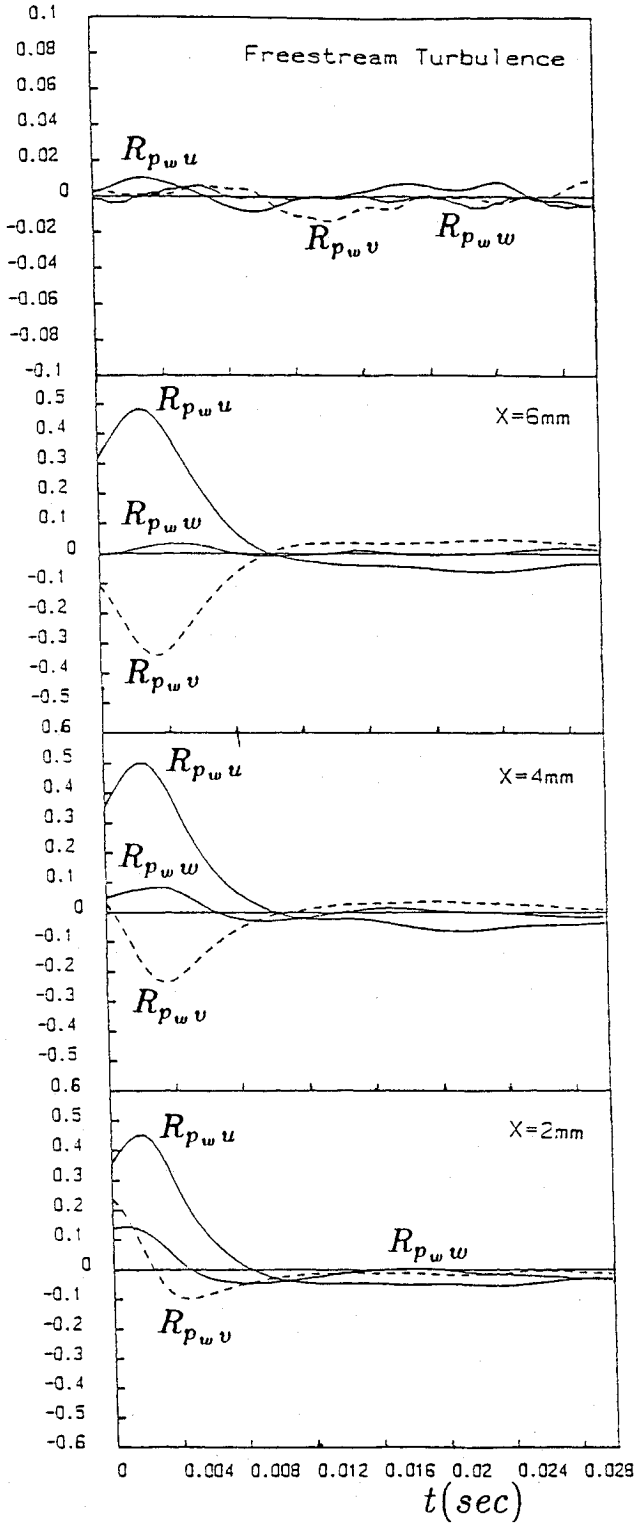


**Fig. 6 Distributions of $R_{p_w u}(\Delta x, 0, 0, \Delta t)$, $R_{p_w v}(\Delta x, 0, 0, \Delta t)$, and $R_{p_w w}(\Delta x, 0, 0, \Delta t)$ for arrangement II at $U_0 = 9.6$ m/s, where $p_w$ was measured at $y = 16$ mm over the surface of the plate, and the $x$-type probe was mounted at $x = 2$, 4, and 6 mm, and at the freestream, respectively.**

neous velocity vector are denoted as $\tilde{U} = (U + u)\hat{i}$, $\tilde{V} = (V + v)\hat{j}$, and $\tilde{W} = w\hat{k}$, respectively. Equation (2) can be expanded into

$$\frac{\tilde{P}}{\rho} + \frac{p}{\rho} + \frac{1}{2}(U + u)^2 + \frac{1}{2}(V + v)^2 + \frac{1}{2}w^2 = \frac{P_0}{\rho} \tag{3}$$

Taking the time average over Eq. (3), one obtains

$$\frac{P}{\rho} + \frac{1}{2}U^2 + \frac{1}{2}V^2 + \frac{1}{2}\overline{u^2} + \frac{1}{2}\overline{v^2} + \frac{1}{2}\overline{w^2} = \frac{P_0}{\rho} \tag{4}$$

Subtracting Eq. (4) from Eq. (3) one obtains

$$\frac{p}{\rho} + Uu + \frac{1}{2}u^2 + Vv + \frac{1}{2}v^2 + \frac{1}{2}w^2 - \left(\frac{1}{2}\overline{u^2} + \frac{1}{2}\overline{v^2} + \frac{1}{2}\overline{w^2}\right) = 0 \tag{5}$$

In the region of interest, i.e., $2 < x < 6$ mm and $8 < y < 20$ mm of the present flow, the value of $V$ measured is found to be larger than the value of $U$ measured by about two to six times in magnitude. Furthermore, in view of the fact that for arrangements I–V the turbulence intensities of $u$, $v$, and $w$ measured are of the same order and are no more than 10% of $U_0$, the term $\frac{1}{2}u^2 + \frac{1}{2}v^2 + \frac{1}{2}w^2 - (\frac{1}{2}\overline{u^2} + \frac{1}{2}\overline{v^2} + \frac{1}{2}\overline{w^2})$ can be neglected in comparison with the term of $Uu + Vv$. Thus, one obtains

$$(p/\rho) + Uu + Vv \approx 0 \tag{6}$$

It should be noted that the expression of Eq. (6) is not quite true for the case of arrangement VI, for which the freestream turbulence intensity measured exceeds 10% of $U_0$.

Because the signs of $u$ and $v$ are opposite to each other for most of the time measured, one first considers the case when $u$ is positive and $v$ is negative. Then,

$$Uu + Vv < 0 \tag{7}$$

where $U$ is negative and $V$ is positive in the positive $y$ direction. Consequently, Eq. (6) implies that

$$p > 0 \tag{8}$$

On the other hand, if $u$ is negative and $v$ is positive, then Eq. (6) implies that

$$p < 0 \tag{9}$$

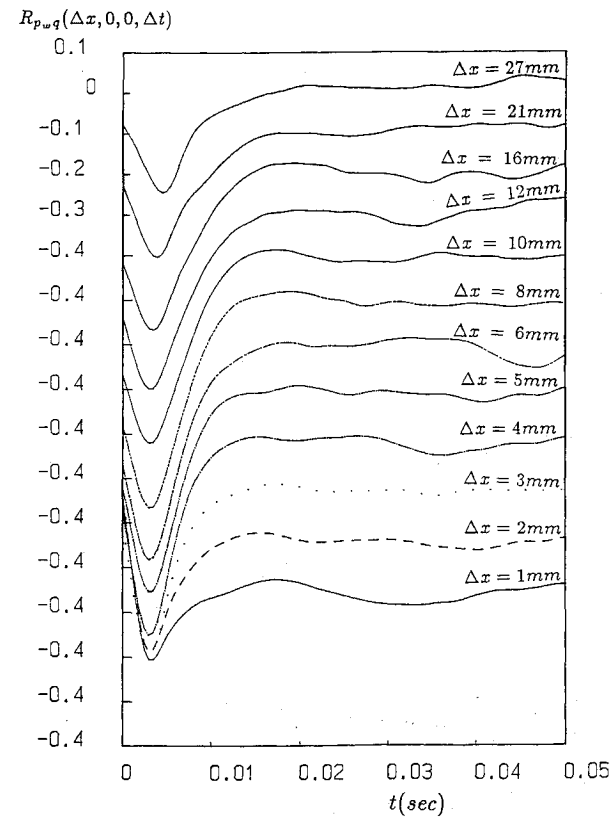


**Fig. 7 Set of distributions of $R_{p_w q}(\Delta x, 0, 0, \Delta t)$ for $x = 1 \sim 27$ mm, for arrangement II, $U_0 = 9.6$ m/s and $y = 16$ mm.**

The expressions of Eqs. (6–9) infer that the sign of $p$ is the same as that of $u$ but is opposite to that of $v$. These findings are noted to have the same behaviors as those of $p_w(t + \tau_{opt})u(t)$ and $p_w(t + \tau_{opt})v(t)$ shown in Fig. 6. Hence, a further postulation is that the pressure fluctuations $p$ accompanied with the velocity fluctuations can be correlated with the wall-pressure fluctuations $p_w$ through a time lag relation.

### D. Normalization of the Optimal Time Delay

Figure 7 presents the distributions of $R_{p_w q}(\Delta x, 0, 0, \Delta t)$ obtained with a normal hot wire situated in a region of $x = 1$–$27$ mm, at $y = 16$ mm and $U_0 = 9.6$ m/s, for arrangement II. In each of the distributions shown, a negative peak value is observed that corresponds to the occurrence of $R_{p_w q}(\Delta x, 0, 0, \tau_{opt})$. This behavior resembles that of $R_{p_w v}(\Delta x, 0, 0, \tau_{opt})$ mentioned previously. An explanation for this is that in the region near the normal plate the value of $V$ measured is larger than the value of $U$ measured by about two to six times in magnitude, thus the sign of $R_{p_w q}(\Delta x, 0, 0, \Delta t)$ is likely to be the same as that of $R_{p_w v}(\Delta x, 0, 0, \Delta t)$. The distributions of $R_{p_w q}(\Delta x, 0, 0, \Delta t)$ in Fig. 7 together with those obtained for the cases of $U_0 = 5.0$ and 7.6 m/s at $y = 8$, 12, 16, and 20 mm not shown here indicate a trend in common: that for a fixed freestream velocity the value of $\tau_{opt}$ is found to increase with the separation distance of $\Delta x$. This trend can be illustrated by

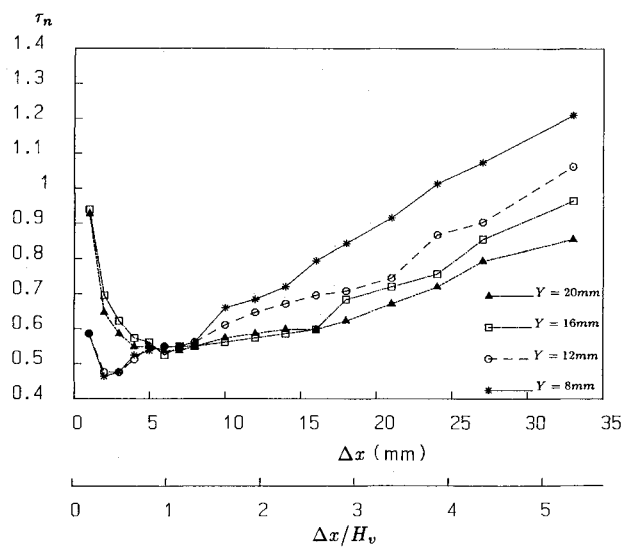


**Fig. 8 Distributions of the nondimensionalized optimal time delay $\tau_n$ at $U_0 = 5.0$ m/s for arrangement II.**

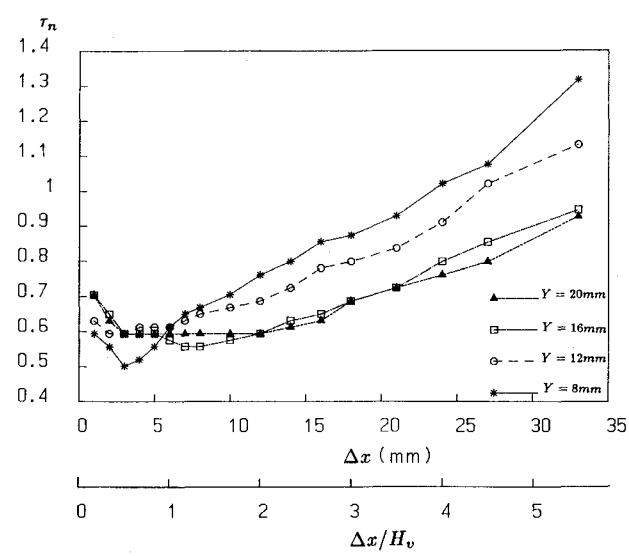


**Fig. 9 Distributions of the nondimensionalized optimal time delay $\tau_n$ at $U_0 = 7.6$ m/s for arrangement II.**

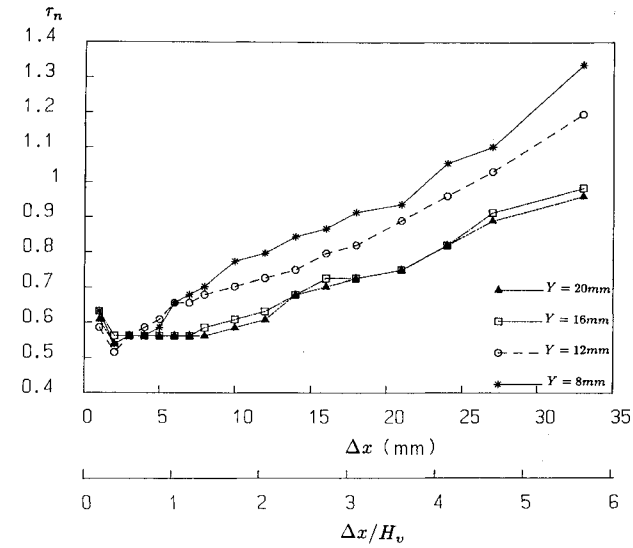


**Fig. 10 Distributions of the nondimensionalized optimal time delay $\tau_n$ at $U_0 = 9.6$ m/s for arrangement II.**

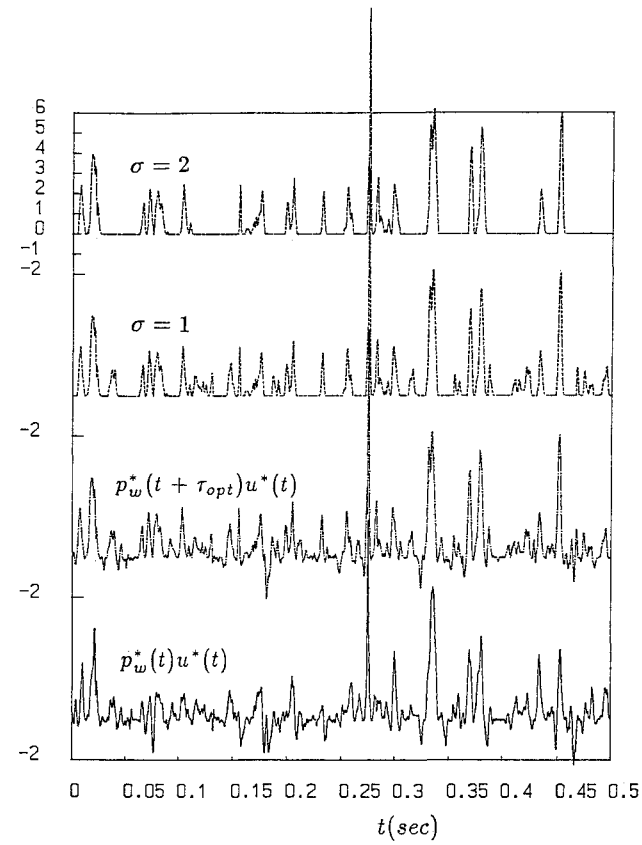


**Fig. 11 Typical time traces of $p_w^*(t)u^*(t)$, $p_w^*(t + \tau_{opt})u^*(t)$, and the qualified intermittent signals of $p_w^*(t + \tau_{opt})u^*(t)$ subject to the threshold conditions of $\sigma = 1$ and 2, respectively, at $U_0 = 7.6$ m/s for arrangement II at $x = 4$ mm and $y = 16$ mm.**

a plot of the nondimensional quantity $\tau_n$ vs the normalized distance of the hot-wire probe from the wall surface $\Delta x/H_v$. Here,

$$\tau_n = \frac{\tau_{opt} U_0}{W_d} \tag{10}$$

The distributions of $\tau_n$ vs $\Delta x/H_v$ for arrangement II, at $U_0 = 5.0$, 7.6, and 9.6 m/s, are shown in Figs. 8, 9, and 10, respectively. An interesting feature revealed from Figs. 8–10 is that the minimal value of $\tau_n$ seen in each figure occurred in the neighborhood of $\Delta x \approx H_v$. Referring to Wei and Miau,[10] the

location of $x = H_v$ signifies the nearest position at which the stretched vortical structures can approach the normal plate; thus it is reasonable that the minimal value of $\tau_n$ is obtained at this location. For $\Delta x > H_v$, $\tau_n$ increases almost linearly with $\Delta x$, implying that the pressure fluctuations sensed at the wall are associated with the disturbance embedded in the mean flow convecting toward the wall. It is also noted in Figs. 8–10 that the slope of the distribution of $\tau_n$ vs $\Delta x/H_v$ decreases as $y$ increases. This is attributed to the fact that the convection speed of the flow increases as the measured section gets farther away from $y = 0$. No satisfactory explanation is found for the trend that the values of $\tau_n$ increase in the region very close to the wall, which could be due to the viscous effect that causes the phase variations of the velocity fluctuation in this region.

### E. Intermittent Characteristics of $p_w^*(t + \tau_{opt})u^*(t)$

The unsteady characteristics of the flow structures in the stagnation region can be examined with the time traces of velocity-pressure cross correlation. Figure 11 compares a set of the instantaneous traces of $p_w^*(t)u^*(t)$ and $p_w^*(t+\tau_{opt})u^*(t)$ for the hot-wire probe located at $x = 4$ mm and $y = 16$ mm, and $p_w$ is measured at $y = 16$ mm and $U_0 = 7.6$ m/s for arrangement II. This figure shows that the positive peak values observed in the time trace of $p_w^*(t + \tau_{opt})u^*(t)$ appear to be more pronounced than those in the time trace of $p_w^*(t)u^*(t)$, inferring that the fluctuations in the traces of $u^*(t)$ and $p_w^*(t + \tau_{opt})$ are tuned with a time shift of $\tau_{opt}$. Furthermore, to select the intermittent events of large positive peak values in the time trace of $p_w^*(t + \tau_{opt})u^*(t)$ a detection function $D(t)$ is employed,

$$D(t) = \begin{cases} 1, & \text{if } M_{p_w u}^* > \sigma \\ 0, & \text{otherwise} \end{cases} \tag{11}$$

In Eq. (11), $M_{p_w u}^* = p_w^*(t + \tau_{opt})u^*(t)$, and $\sigma$ denotes a threshold value to be specified. Two traces of $M_{p_w u}^* D(t)$ that are subject to the threshold conditions of $\sigma = 1$ and 2 are presented in Fig. 11. A comparison of the time traces of $M_{p_w u}^*$ and $M_{p_w u}^* D(t)$ indicates that the events of large variations in the time trace of $M_{p_w u}^*$ survive for further analysis. The number of events per unit time obtained from a trace of $M_{p_w u}^* D(t)$ is then denoted as $f_q$. Generally speaking, the value of $f_q$ obtained is dependent on the threshold condition of $\sigma$ specified. Chen and Blackwelder[14] found that whenever a simple threshold condition is applied to a function that has a continuous probability distribution, the statistics of the qualified events vary monotonically with the threshold parameter.

**Table 2 Statistics of occurrences and time duration of the qualified events in the time trace of $p_w^*(t + \tau_{opt})u^*(t)$ with the threshold condition of $\sigma = 1$[a]**

| Arrangement | $Re$ | $f_q \pm \Delta f_q$, 1/s | $t_q \pm \Delta t_q$, s | $f_q^*$ | $t_q^*$ |
|---|---|---|---|---|---|
| I | $2.5\times10^4$ | $29.05\pm3.42$ | $0.01298\pm0.00104$ | 1.92 | 5.10 |
| I | $3.2\times10^4$ | $41.60\pm3.76$ | $0.00840\pm0.00048$ | 2.04 | 5.83 |
| II | $1.66\times10^4$ | $28.20\pm3.13$ | $0.01302\pm0.00073$ | 1.96 | 5.33 |
| II | $2.5\times10^4$ | $46.60\pm3.33$ | $0.00886\pm0.00046$ | 2.11 | 5.11 |
| II | $3.2\times10^4$ | $63.07\pm3.49$ | $0.00683\pm0.00029$ | 2.29 | 5.33 |
| III | $1.0\times10^4$ | $17.90\pm1.45$ | $0.01851\pm0.00144$ | 1.65 | 4.98 |
| III | $1.66\times10^4$ | $37.13\pm2.69$ | $0.00988\pm0.00074$ | 2.09 | 5.70 |
| III | $2.5\times10^4$ | $60.73\pm3.75$ | $0.00628\pm0.00044$ | 2.06 | 5.39 |
| III | $3.2\times10^4$ | $74.20\pm5.89$ | $0.00541\pm0.00040$ | 1.98 | 4.92 |
| IV | $2.5\times10^4$ | $52.27\pm3.72$ | $0.00780\pm0.00060$ | 1.98 | 4.85 |
| IV | $3.2\times10^4$ | $69.07\pm5.23$ | $0.00606\pm0.00050$ | 1.96 | 4.68 |
| V | $1.66\times10^4$ | $42.92\pm2.60$ | $0.01024\pm0.00050$ | 1.81 | 4.12 |
| V | $2.5\times10^4$ | $67.07\pm4.61$ | $0.00710\pm0.00030$ | 2.19 | 4.61 |
| V | $3.2\times10^4$ | $76.47\pm5.99$ | $0.00539\pm0.00020$ | 2.11 | 5.12 |
| VI | $1.0\times10^4$ | $23.07\pm2.60$ | $0.01323\pm0.00101$ | 1.10 | 3.59 |
| VI | $1.66\times10^4$ | $44.13\pm2.63$ | $0.00815\pm0.00057$ | 1.47 | 4.05 |
| VI | $2.5\times10^4$ | $64.53\pm3.78$ | $0.00567\pm0.00045$ | 1.42 | 3.89 |
| VI | $3.2\times10^4$ | $81.27\pm4.78$ | $0.00476\pm0.00029$ | 1.44 | 3.72 |

[a]The 95% confidence intervals of $f_q^*$ and $t_q^*$ with respect to the mean values of arrangements I–V are about 15 and 14%, respectively.

**Table 3 Statistics of occurrences and time duration of the qualified events in the time trace of $p_w^*(t + \tau_{opt})u^*(t)$ with the threshold condition of $\sigma = 2$[a]**

| Arrangement | $Re$ | $f_q \pm \Delta f_q$, 1/s | $t_q \pm \Delta t_q$, s | $f_q^*$ | $t_q^*$ |
|---|---|---|---|---|---|
| I | $2.5\times10^4$ | $13.46\pm2.16$ | $0.01483\pm0.00115$ | 0.89 | 4.47 |
| I | $3.2\times10^4$ | $18.93\pm2.38$ | $0.00976\pm0.00060$ | 0.93 | 5.02 |
| II | $1.66\times10^4$ | $12.07\pm1.80$ | $0.01409\pm0.00106$ | 0.84 | 4.92 |
| II | $2.5\times10^4$ | $22.99\pm1.92$ | $0.01040\pm0.00058$ | 1.04 | 4.36 |
| II | $3.2\times10^4$ | $32.01\pm2.51$ | $0.00807\pm0.00042$ | 1.16 | 4.51 |
| III | $1.0\times10^4$ | $8.30\pm1.24$ | $0.02153\pm0.00204$ | 0.77 | 4.28 |
| III | $1.66\times10^4$ | $18.00\pm1.96$ | $0.01151\pm0.00099$ | 1.01 | 4.89 |
| III | $2.5\times10^4$ | $27.87\pm2.32$ | $0.00727\pm0.00063$ | 0.94 | 4.66 |
| III | $3.2\times10^4$ | $33.47\pm2.60$ | $0.00645\pm0.00054$ | 0.89 | 4.12 |
| IV | $2.5\times10^4$ | $26.60\pm2.83$ | $0.00913\pm0.00075$ | 1.01 | 4.14 |
| IV | $3.2\times10^4$ | $34.67\pm2.93$ | $0.00705\pm0.00052$ | 0.98 | 4.02 |
| V | $1.66\times10^4$ | $21.58\pm1.82$ | $0.01202\pm0.00070$ | 0.91 | 3.51 |
| V | $2.5\times10^4$ | $35.07\pm2.98$ | $0.00813\pm0.00049$ | 1.14 | 4.01 |
| V | $3.2\times10^4$ | $36.87\pm4.34$ | $0.00627\pm0.00026$ | 1.03 | 4.44 |
| VI | $1.0\times10^4$ | $11.07\pm1.98$ | $0.01531\pm0.00139$ | 0.53 | 3.10 |
| VI | $1.66\times10^4$ | $21.00\pm2.09$ | $0.00987\pm0.00093$ | 0.69 | 3.37 |
| VI | $2.5\times10^4$ | $30.47\pm2.78$ | $0.00670\pm0.00068$ | 0.67 | 3.29 |
| VI | $3.2\times10^4$ | $37.93\pm2.93$ | $0.00576\pm0.00048$ | 0.67 | 3.11 |

[a]The 95% confidence intervals of $f_q^*$ and $t_q^*$ with respect to the mean values of arrangements I–V are about 18.5 and 16%, respectively.

Hence, it is not meaningful to pursue an absolute value of $f_q$ in the present study. Instead, a strategy adopted is to compare the values of $f_q$ that are obtained under different experimental conditions but that refer to a fixed threshold value of $\sigma$.

In addition to the quantity of $f_q$ obtained, the average time duration of these qualified events, denoted as $t_q$, can also be obtained through the detection procedure.

The statistics of $f_q$ and $t_q$ and the 95% confidence interval[11,15] corresponding to the threshold conditions of $\sigma = 1$ and 2 for arrangements I–VI are listed in Tables 2 and 3, respectively.

An analysis of the parameters influencing the quantities of $f_q$ and $t_q$ gives the following functional forms:

$$f_q = F(W_d, U_0, u_0, L_x, x, y, \nu, \rho) \tag{12}$$

$$t_q = G(W_d, U_0, u_0, L_x, x, y, \nu, \rho) \tag{13}$$

The expressions of Eqs. (12) and (13) can be simplified based on the following considerations: 1) Since the geometry of the normal plate is fixed in these experiments, the parameter of $W_d$ is constant in the present analysis; 2) Since the stretched vortical structures are situated mainly outside the boundary layer,[2,10,11] the effect of viscosity in Eqs. (12) and (13) does not play a role in the present analysis; 3) Since the present flow is incompressible, the density of the fluid is considered as a constant; and 4) Since the stretched vortices near the normal plate are basically aligned in the $y$ direction and extend over a certain region away from the mean stagnation streamline (see Fig. 4, for example), it is assumed that $f_q$ and $t_q$ are weakly dependent on $x$ and $y$ if the measured region is properly chosen in the neighborhood of $x = H_v$ and $6 < y < 16$ mm. Finally, it arrives at

$$f_q = F(U_0, u_0, L_x) \tag{14}$$

$$t_q = G(U_0, u_0, L_x) \tag{15}$$

The previous study[10] showed that $L_x$ plays an important role in influencing the characteristic size of the stretched vortical structures. The intensity of freestream turbulence is known to be crucial to the development of velocity fluctuation in the stagnation region.[3,8,9] The parameter of $U_0$ was found to have an effect on the convection of turbulence eddies toward the stagnation region; however, later it is realized that this parameter is not independent of $u_0$. Finally, it is suggested that $f_q$ and

$t_q$ be scaled with the parameters of $L_x$ and $u_0$, and are arranged in the following forms:

$$f_q^* = (f_q L_x / u_0) \tag{16}$$

$$t_q^* = (L_x / t_q u_0) \tag{17}$$

Traci and Wilcox[16] also pointed out that $L_x$ and $u_0$ are the major parameters characterizing the freestream turbulence and should be incorporated into the turbulence model for the computation of the turbulent stagnation flow.

The normalized values of $f_q^*$ and $t_q^*$ for arrangements I–VI that correspond to the threshold conditions of $\sigma = 1$ and 2 are shown in Tables 2 and 3, respectively, and appear consistent. Table 2 shows that when $\sigma = 1$, the mean values of $f_q^*$ and $t_q^*$ are about 2.0 and 5.1, respectively. Table 3 shows that when $\sigma = 2$, the mean values of $f_q^*$ and $t_q^*$ are about 0.96 and 4.4, respectively. The success of normalization with the expressions of Eqs. (16) and (17) shows that $L_x$ and $u_0$ are appropriate for scaling $f_q$ and $t_q$.

The discrepancy noted between the values of $f_q^*$ and $t_q^*$ in Tables 2 and 3 is attributed to the fact that, for $\sigma = 1$, the events corresponding to the flow structures of smaller scales and lower fluctuation intensity could be included for the statistics, whereas for $\sigma = 2$ only the events of higher intensity are counted. However, it should be mentioned that both threshold conditions of $\sigma = 1$ and 2 can successfully ignore the fluctuations associated with the background turbulence in the raw trace of the velocity-pressure correlation.

Note that in Tables 2 and 3 the values of $f_q^*$ and $t_q^*$ for the arrangement VI appear to deviate somewhat from those of the arrangements I–V. This deviation is noted because in the case of arrangement VI the freestream turbulence produced is characterized by high intensity and is far from homogeneous at the location of the normal plate.

## V. Concluding Remarks

This work is focused on the relationship between the velocity fluctuations measured near the normal plate and the pressure fluctuations on the wall. The correlation measurements obtained indicate that the optimal time delay between these two fluctuation quantities measured can be explained by the effect of mean-flow convection, which further implies that wall-pressure fluctuations measured are induced by the stretched vortical structures developed in the stagnation region. Conditional sampling analysis of the time traces of pressure-velocity correlation unveils the unsteady characteristics of the stretched vortical structures developed in the stagnation region. The statistics for the number of the intermittent events per unit time and the average time duration of the stretched vortical structures detected at a point near the wall can be successfully scaled by the turbulence intensity and the integral length scale of the freestream turbulence.

## Acknowledgments

This work was supported by the National Science Council, Republic of China, under Contact NSC80-0401-E006-35. The authors would like to thank Y. C. Chao for kindly lending us the Bruel & Kjaer microphone system.

## References

[1]Kestin, J., "The Effect of Free Stream Turbulence on Heat Transfer Rates," *Advances in Heat Transfer,* Vol. 3, 1966, pp. 1–32.

[2]Sadeh, W. Z., and Brauer, H. J., "A Visual Investigation of Turbulence in Stagnation Flow about a Circular Cylinder," *Journal of Fluid Mechanics,* Vol. 99, Pt. 1, 1980, pp. 53–64.

[3]Nagib, H. M., and Hodson, P. R., "Vortices Induced in a Stagnation Region by Wakes," *Aerodynamic Heating and Thermal Protection Systems,* edited by L. S. Fletcher, Vol. 59, Progress in Aeronautics and Astronautics, AIAA, New York, 1977, pp. 66–90.

[4]Sadeh, W. Z., Sutera, S. P., and Maeder, P. F., "Analysis of Vorticity Amplification in the Flow Approaching a Two-Dimensional Stagnation Point," *Zeitschrift fuer Angewandte Mathematik und Physik,* Vol. 21, 1970a, pp. 699–716.

[5]Sadeh, W. Z., Sutera, S. P., and Maeder, P. F., "An Investigation of Vorticity Amplification in Stagnation Flow," *Zeitschrift fuer Angewandte Mathematik und Physik,* Vol. 21, 1970b, pp. 717–742.

[6]Hunt, J. C. R., "A Theory of Turbulent Flow Round Two-Dimensional Bluff Bodies," *Journal of Fluid Mechanics,* Vol. 61, Pt. 4, 1973, pp. 625–706.

[7]Batchelor, G. K., and Proudman, I., "The Effect of Rapid Distortion of a Fluid in Turbulent Motion," *Quarterly Journal of Mechanics and Applied Mathematics,* Vol. 7, Pt. 1, 1954, pp. 83–103.

[8]Bearman, P. W., "Some Measurements of the Distortion of Turbulence Approaching a Two-Dimensional Bluff Body," *Journal of Fluid Mechanics,* Vol. 53, Pt. 3, 1972, pp. 451–467.

[9]Britter, R. E., Hunt, J. C. R., and Mumford, J. C., "The Distortion of Turbulence by a Circular Cylinder," *Journal of Fluid Mechanics,* Vol. 92, Pt. 2, 1979, pp. 269–301.

[10]Wei, C. Y., and Miau, J. J., "Stretching of Freestream Turbulence in Stagnation Region," *AIAA Journal,* Vol. 30, No. 9, 1992, pp. 2196–2203.

[11]Wei, C. Y., "Mechanism of Vorticity Stretching in Stagnation Region," Ph.D. Thesis, National Cheng-Kung Univ., Tainan, Taiwan, ROC, 1992.

[12]Tan-Atichat, J., Nagib, H. M., and Loehrke, R. I., "Interaction of Free-Stream Turbulence with Screens and Grids: A Balance Between Turbulence Scales," *Journal of Fluid Mechanics,* Vol. 114, Jan. 1982, pp. 501–528.

[13]Taulbee, D. B., and Tran, L., "Stagnation Streamline Turbulence," *AIAA Journal,* Vol. 26, No. 8, 1988, pp. 1011–1013.

[14]Chen, C. H. P., and Blackwelder, R. F., "Large-Scale Motion in a Turbulent Boundary Layer: A Study Using Temperature Contamination," *Journal of Fluid Mechanics,* Vol. 89, Pt. 1, 1978, pp. 1–31.

[15]Bendat, J. S., and Piersol, A. G., *Random Data: Analysis and Measurement Procedures,* Wiley, New York, 1971.

[16]Traci, R. M., and Wilcox, D. C., "Freestream Turbulence Effect on Stagnation Point Heat Transfer," *AIAA Journal,* Vol. 13, No. 7, 1975, pp. 890–896.